Magnetic structure of MnSi under an applied field probed by polarized small-angle neutron scattering

S. V. Grigoriev,[1] S. V. Maleyev,[1] A. I. Okorokov,[1] Yu. O. Chetverikov,[1] P. Böni,[2] R. Georgii,[2] D. Lamago,[2] H. Eckerlebe,[3] and K. Pranzas[3]

[1]*Petersburg Nuclear Physics Institute, Gatchina, St. Petersburg 188350, Russia*

[2]*Physics Department E21/ZWE FRM-II, Technische Universität München, 85747 Garching, Germany*

[3]*GKSS Forschungszentrum, 21502 Geesthacht, Germany*

(Received 19 June 2006; revised manuscript received 20 October 2006; published 14 December 2006)

The magnetic structure of a single crystal MnSi under applied field has been studied by small angle diffraction with polarized neutrons below $T_C=28.7$ K. Experiments have shown that in zero field the magnetic structure of MnSi consists of four left-handed spiral domains oriented along four $\langle 111\rangle$ axes. The magnetic field, applied along one of the $\langle 111\rangle$ axes, produces a single domain helix oriented along the field at $H_{C1} \approx 80$ mT at low temperatures. The magnetic mosaic of the spin structure changes with the magnetic field and has a maximum at H_{C1}. The integral intensity of the Bragg reflection shows a sharp minimum at $H_{in} \approx 160$ mT attributed to an instability of the helix structure. When the field has a component perpendicular to the helix wave vector **k**, it rotates toward the field direction in the field range $H<H_{in}$. Additionally, a second harmonic of the helix structure is induced by the perpendicular magnetic field for $H<H_{in}$. These three features are well explained accounting for the presence of a spin wave gap $\Delta \sim g\mu_B H_{in}/\sqrt{2} \simeq 12$ μeV, which provides the stability of the spin wave spectrum with respect to the perpendicular magnetic field. Further increase of the field leads to a magnetic phase transition from conical to a ferromagnetic state near $H_{C2} \approx 600$ mT. The critical field H_{C2} is related to the spin wave stiffness A as $g\mu_B H_{C2}=Ak^2$. Our findings are in agreement with the recently developed theory [Phys. Rev. B **73**, 174402 (2006)] for cubic magnets with Dzyaloshinskii-Moriya interaction, which relates the major parameters of the spin wave spectrum (such as the spin wave stiffness and the gap) with the features of the spin structure of MnSi being observed under applied magnetic field.

DOI: 10.1103/PhysRevB.74.214414 PACS number(s): 75.25.+z, 61.12.Ex

I. INTRODUCTION

The weak itinerant ferromagnet MnSi orders below $T_C=29$ K in a left-handed spin helical structure with a propagation vector $(2\pi/a)(\xi,\xi,\xi)$ with $\xi=0.017$.[1,2] The helicity is induced by an antisymmetric Dzyaloshinskii-Moriya (DM) exchange interaction caused by the lack of a center of symmetry in Mn atomic arrangement.[3–5] This DM interaction is isotropic in cubic crystals, however, a weak anisotropic exchange (AE) interaction fixes the direction of the magnetic spiral below T_C along the cube diagonals $\langle 111\rangle$.[4] Although the magnetic properties of MnSi under applied magnetic field were studied in detail by different methods,[6–9] up to now they remained puzzling due to lack of a microscopic quantitative description of the obtained experimental results. In particular, the nonlinear behavior of the magnetic susceptibility with a small upturn curvature in the range of small field $H \leqslant 150$ mT has not been explained yet.[6] The nature of A phase observed in the vicinity of T_C under applied field was not clarified too.[7–9]

The neutron scattering experiments[1] showed that the magnetic helical structure becomes a single-domain conical structure in a magnetic field $H_{C1} \simeq 80$ mT at low temperature. The cone angle α decreases as the field increases and an induced ferromagnetic state appears at $H_{C2} \simeq 600$ mT with the saturated magnetic moment of 0.4 μ_B per Mn atom. This value of the moment is much smaller than the effective paramagnetic moment above T_C, which has been estimated to be 1.4 μ_B from susceptibility measurements.[2] As was also shown in Ref. 1, if the direction of the applied magnetic field **H** is not collinear to one of the $\langle 111\rangle$, the helix wave vector **k** rotates toward the magnetic field. The period of the helix does not change with the field. The **k**-rotation effect was theoretically treated by Plumer and Walker on the basis of a phenomenological approach.[10,11]

Bearing in mind a long period of the spin density wave of order of 18 nm, small angle neutron scattering (SANS) gives the unique opportunity to study the magnetic structure of MnSi. The use of the polarized neutrons is especially important because of the presence of a chiral (axial) vector in the system. As shown in Refs. 12 and 13 the presence of such an axial vector, or single-handed helicity, leads to the appearance of a polarization dependent contribution in the neutron scattering cross section. Indeed, the first experiments with polarized neutrons[14–16] demonstrated that the scattering is strongly polarization dependent and therefore the spin helix in MnSi is single-handed one. However, a thorough study of the temperature and magnetic field dependence of the chirality in this system has not been done yet.

Recently, the magnetic properties of MnSi have attracted much attention because of the discovery of a quantum phase transition to a magnetically disordered state that is easily reached under applied pressure. As was found in Refs. 17–19, the critical temperature T_C decreases with increasing pressure and the long range magnetic order disappears at $T=0$ and a critical pressure of $p_C \approx 14.6$ kbar. Another interesting feature of the magnetic structure of MnSi is observed near the critical temperature in an applied magnetic field. A structural spin instability, called A phase, was found in the field range from $H_{A1} \sim 130$ mT to $H_{A2} \sim 200$ and slightly

below T_C by measuring the magnetization and magnetoresistance.[7] The neutron scattering experiments have shown that the intensity of the Bragg reflections, with helix wave vector oriented along the field, decreases strongly in a narrow range $H \sim H_A$ near T_C (Ref. 8). AC susceptibility measurements under applied pressure have confirmed the presence of this instability near T_C in a field from H_{A1} to H_{A2} (Ref. 9). It was also found that while T_C drops rapidly with increasing pressure, absolute values of the characteristic fields H_{C1}, H_{C2} and H_{A1}, H_{A2} do not change significantly.

Recently the magnetic structure of MnSi was studied by small angle polarized neutron scattering near $T_C=29$ K under applied field.[20] The weak magnetic field applied along the [111] axes removes the domain walls and creates a single domain sample with the helix wave vector along the field. The 90° reorientation of the spin spiral from the [111] axis to the $[1\bar{1}0]$ axis is observed for $130<H<180$ mT near T_C. Further increase of the field above 180 mT restores the original orientation of the helix and leads to an induced ferromagnetic state at 350 mT. This observation clarifies the nature of the structural spin instability found in the H-T phase diagram of MnSi by other techniques.[7–9] We explain this phenomenon as a result of the spin-wave Bose condensation provoked by the field perpendicular to the helix axis.[21]

In this paper we present results of SANS measurements with polarized neutrons of the magnetic structure in MnSi under applied field well below T_C. Neutron scattering experiments have shown a number of features attributed first to the process of reorientation of helices from the multidomain structure to the single domain structure at $H=H_{C1}$; second, to the structural instability of the helix around $H_{in}=160$ mT; and third, to the field-induced phase transition from the conical to the ferromagnetic state at H_{C2}. On the basis of our findings we have examined a theory recently developed for the cubic magnets with Dzyaloshinskii-Moriya interaction, which suggests the presence of the small gap in the spin wave spectrum of MnSi.[21] Particularly, the phenomena observed in our experiments allowed to estimate the gap as being of the order of 12 μeV.

The similar phenomena, i.e., rotation of the magnetic ordering wave vector of a DM spiral and generation of higher harmonics when spiral is bunched by the magnetic field, were studied in detail in Refs. 22 and 23 for quasiantiferromagnetic (AFM) spiral in $Ba_2CuGe_2O_7$. The authors of Refs. 22 and 23 have generalized the spin wave description of slightly distorted exchange spiral, which was developed in an earlier paper[24] to the case of a DM spiral and have obtained a consistent and comprehensive description of the spin structure and spin excitations in quasi-AFM DM spiral in $Ba_2CuGe_2O_7$. The authors have observed the spin wave gap related to the single-ion easy-plane anisotropy, which appears due to the DM interaction considered as a second order perturbation.[25–28] However, in case of the cubic symmetry this correction can not produce a spin-wave gap as it has a form of a small correction to the isotropic exchange.

The paper is organized in the following way. Section II summarizes the essence of the theory developed in Ref. 21. Section III describes the sample, the experimental setup, and the geometry of the experiment. The results of the polarized SANS experiments are shown in Sec. IV. This section is split into three parts each of them dealing with a particular phenomenon under study. In Sec. IV A the mosaic of the helix structure and the integral intensity of the Bragg reflection under field applied along the [111] axis is studied. In Sec. IV B the **k**-rotation effect is studied for two different orientations of the applied magnetic field: $H\|[100]$ and $H\|[110]$. The process of **k** rotation is accompanied by the appearance of the second harmonic of the helix spin structure as soon as a field component perpendicular to the helix wave vector occurs (Sec. IV C). Section V is devoted to the temperature evolution of the helix structure. Section VI contains a summary of the obtained results. The phenomena mentioned above are interpreted in terms of the theory developed in Ref. 21 and corresponding parameters for the interactions driving the magnetic system of MnSi are obtained.

II. THEORETICAL BACKGROUND

A theory was recently developed by one of the authors to describe properties of cubic helical magnets with DMI.[21] The following interactions are taken into account in this theory: conventional isotropic exchange A, DM interaction D, AE interaction F, magnetic dipolar interaction $\omega_0=g\mu_B/a^3$ where a is the lattice constant, Zeeman energy $g\mu_B H$ and cubic anisotropy K. The ground state energy and the spin wave spectrum were evaluated taking into account that DM interaction and anisotropic interactions are of the first and of the second order in the spin-orbit interaction. So we have a hierarchy of interactions in the system: $A \gg Da \gg F$, Ka^2, $\omega_0 a^2$ where A is the spin-wave stiffness in the exchange approximation. It is well known[3–5] that DMI is responsible for the magnetic helix structure with the wave vector

$$k = D/A. \tag{1}$$

In cubic crystals the DMI fixes the sense of the helix (right or left handed) but does not determine its direction. It is stabilized by a very weak AE interaction and cubic anisotropy. It is shown in Refs. 4 and 21 that in the absence of a field the classical energy for orientation of the helix vector **k** is given by

$$E_{cl} = f_{an}^0 \sum_{i=x,y,z} \hat{c}_i^2 (\hat{a}_i^2 + \hat{b}_i^2), \tag{2}$$

where $f_{an}^0 = \frac{S^2 F k^2}{4} - \frac{3S^4 K}{8}$, where F and K are the anisotropic exchange and the cubic anisotropy constants, respectively. $\hat{a}$, $\hat{b}$, and $\hat{c}$ are mutually perpendicular unit vectors describing the helix: $\hat{c}$ is parallel to the helix wave vector **k**, and $\hat{a}$, $\hat{b}$ are in the plane of the spin rotation perpendicular to $\hat{c}$. From this expression one can see that the helix structure along $\langle 111 \rangle$ is realized if $f_{an}^0 < 0$. Otherwise, the structure along $\langle 100 \rangle$ evolves. The helix structure along $\langle 110 \rangle$ is not stable at all.[21]

If the magnetic field is applied along the helix axis $\mathbf{H}\|\mathbf{k}$ the classical energy depends on the product of $H_\|$ and the mean spin induced by the field $S \sin\alpha$, where α is the inclination angle of the spin driven out of the plane perpendicular to **k** by the external field and determined by $\sin\alpha \simeq -H_\|/H_{C2}$ for $H<H_{C2}$ and $\sin\alpha=-1$ for $H>H_{C2}$ where H_{C2} is the

critical field for the transition from the conical spin structure to the ferromagnetic spin state. The critical field is determined by the major interactions as follows:

$$g\mu_B H_{C2} = h_{C2} = Ak^2 + SFk^2/3 \approx Ak^2. \quad (3)$$

One can neglect the second term in Eq. (3) since $A \gg F$. We neglect also small contribution of the dipolar interaction.[21] From Eq. (1) and Eq. (3) one can estimate the major parameters of the magnetic system such as spin wave stiffness $A \approx h_c/k^2$ and the Dzyaloshinskii constant $D = h_c/k$.

If the magnetic field is not parallel to the helix axis ($h < h_{C2}$) the field dependent part of the ground state energy is given by (Ref. 21):

$$E_h = -\frac{Sh_\parallel^2}{2h_{C2}} - \frac{Sh_\perp^2\Delta^2}{2h_{C2}(1+\cos^2\alpha)[\Delta^2 - (h_\perp^2/2)\cos^4\alpha]}. \quad (4)$$

Here $h_\parallel, h_\perp$ are the components of the magnetic field $\mathbf{h} = \mathbf{g}\mu_\mathbf{B}\mathbf{H}$ parallel and perpendicular to the helix wave vector $\mathbf{k}$. The first term of this expression is the magnetic part of the classical energy mentioned above. The second term describes the interaction with the perpendicular field. The spin wave gap Δ is responsible for the stability of the spin configuration in weak perpendicular field. Otherwise the magnetic subsystem is unstable in infinitesimal perpendicular field. As was also shown in Ref. 21 the perpendicular component of the magnetic field deforms the helix structure and gives rise higher harmonics of the spin rotation. The corresponding second-order reflections are observed in this experiment and in Ref. 29.

III. EXPERIMENTAL

A. Sample

A single crystal MnSi was chosen for the study being a disc with a thickness of 2 mm and a diameter of 20 mm. It was cut from a large single crystal that was grown at Ames Laboratory. The lattice constant is $a = 4.558$ Å. The crystallographic mosaicity of the sample was determined on the neutron spectrometer "Reflex" at FZ Julich (Germany). The scans performed show that the average value of the full width half maximum (FWHM) over all measured reflections is 0.22°.

B. Setup

The polarized SANS experiments were carried out at the SANS-2 scattering facility of the FRG-1 research reactor in Geesthacht (Germany). A polarized beam of neutrons with an initial polarization $P_0 = 0.95$, a neutron wavelength $\lambda = 0.58$ nm, a bandwidth $\Delta\lambda/\lambda = 0.1$, and a divergence $\eta = 2.5$ mrad was used, leading to a transverse resolution of 0.75° in a rocking scan. The scattered neutrons were detected by a position sensitive detector with 128×128 pixels. The detector-sample distance was set such that the q range was covered from 6×10^{-2} to 1 nm^{-1} with a step of 0.01 nm^{-1}. The scattering intensity was measured in the temperature range $10 < T \leqslant 30$ K with an accuracy better than 0.05 K. The external magnetic field H from 1 to 800 mT was applied perpendicular to the incident beam and the neutron polarization followed the direction of the magnetic field.

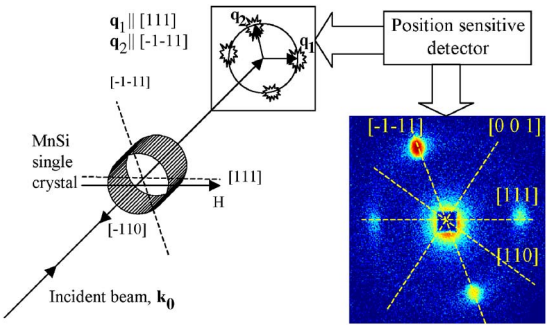

FIG. 1. (Color online) The schematic outline of SAPNS experiment. The single crystal MnSi was oriented such that the incident beam hits the sample along the $[1\bar{1}0]$ axis. Therefore, four crystallographic axes [111], $[11\bar{1}]$, [110], and [001] are laying in the plane perpendicular to the beam direction. The magnetic field **H** and the polarization **P** are applied in the same plane.

C. Geometry of the experiment

The magnetic structure of MnSi in the absence of the field consists of four left-handed spiral domains oriented along the cube diagonals: $\mathbf{k} \| \langle 111 \rangle$. In our experiment, the single crystal was oriented in such a way that two of these axes were set in a plane perpendicular to the incident beam (Fig. 1). These two axes are inclined at about 71° with respect to each other. In the case of the scattering from magnetic spirals with a long period, this geometry allows one to observe diffraction peaks in a range of small-angle scattering, provided that the Bragg condition is fulfilled: $2d\sin(\theta_B/2) = \lambda$, or $q = 2\pi/d$, where d is the period of the spiral and θ_B is the scattering angle. Although the Bragg condition can only be fulfilled for one satellite, due to the large mosaicity of the magnetic structure, the sample can be oriented such that four Bragg reflections can be observed.

The neutron elastic cross section per unit cell of the magnetic helix below T_C has the following form (Ref. 12):

$$\frac{d\sigma}{d\Omega} = \left(\frac{rS}{2}\right)^2 \frac{(2\pi)^3}{V_0}\{[\mathbf{1} + (\hat{q}\hat{c})^2 - 2(\hat{q}\mathbf{P}_0)(\hat{q}\hat{c})]\delta(\mathbf{q} - \mathbf{k}) + [\mathbf{P}_0 \to -\mathbf{P}_0]\delta(\mathbf{q} + \mathbf{k})\}\sin^2\alpha, \quad (5)$$

where $r = 0.54 \times 10^{-12}$ cm, V_0 is the unit cell volume, $\hat{q} = \mathbf{q}/|q|$ is the unit vector of the momentum transfer, $\hat{c}$ is the unit vector of the helix, $\mathbf{P}_0$ is the vector of polarization, α is the cone angle and $\delta(\mathbf{q} \mp \mathbf{k})$ enforce the Bragg conditions.

The second harmonic of the helix structure induced by the perpendicular field is given by (Ref. 21):

$$\frac{d\sigma}{d\Omega} = \left(\frac{rS}{2}\frac{h_\perp}{h_{C2}}\right)^2 \left[\frac{\Delta^2}{\Delta^2 - (g\mu_B h_\perp)^2/2}\right]^2 \times \{[1 + (\hat{c}\hat{q})^2 - 2(\hat{c}\hat{q}) \times (\hat{q}\mathbf{P}_0)]\delta(\mathbf{q} - 2\mathbf{k}) + [\mathbf{P}_0 \to -\mathbf{P}_0]\delta(\mathbf{q} + 2\mathbf{k})\}, \quad (6)$$

where we put $\sin^2\alpha = 1$.

For the single-handed helical structure the neutron cross section depends on the incident polarization $\mathbf{P_0}$. For example

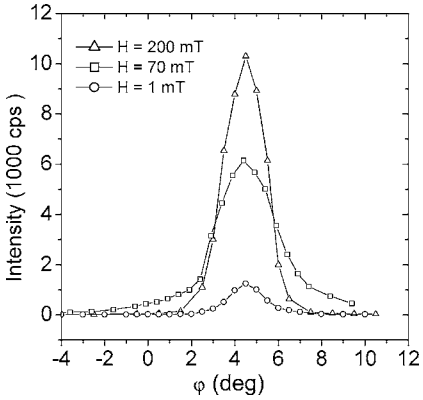

FIG. 2. Angular dependence of the rocking curve of the magnetic Bragg reflection $(\xi\xi\xi)$ at $T=15$ K.

if $\mathbf{P_0}$ is along $\hat{c}$ and $P_0=1$, the scattering is forbidden for $\mathbf{q}=\mathbf{k}$ but is maximal for $\mathbf{q}=-\mathbf{k}$. When $\mathbf{P_0}\perp\hat{\mathbf{c}}$, the scattering does not depend on the polarization. In intermediate case the polarization of the neutron scattering is determined as follows:

$$P=\frac{\sigma(\mathbf{P}_0)-\sigma(-\mathbf{P}_0)}{\sigma(\mathbf{P}_0)+\sigma(-\mathbf{P}_0)}=(\hat{q}\mathbf{P}_0)=\cos\phi, \tag{7}$$

where ϕ is the angle between the incident polarization and the scattering vector. This equation is valid for all measurements presented below for $T<T_C$.

In our experiments the magnetic field and the polarization vector $\mathbf{P}_0$ were set in the plane $[1\bar{1}0]$ (perpendicular to the incident beam) in three different directions of interest: (a) $\mathbf{H}\|\mathbf{P}\|[111]$; (b) $\mathbf{H}\|\mathbf{P}\|[110]$; and (c) $\mathbf{H}\|\mathbf{P}\|[001]$. We investigated experimentally the intensities with the polarization along $[I(q,P_0)]$ and opposite to $[I(q,-P_0)]$ the magnetic field. The measured reflections were characterized by the following quantities: (1) intensity of the peaks: $I_p=[I_p(P)+I_p(-P)]$; (2) polarization of the peaks: $P_p=[I_p(P)-I_p(-P)]/[I_p(P)+I_p(-P)]$; (3) position of the peaks: q_p.

IV. DEPENDENCE ON THE MAGNETIC FIELD

A. Magnetic mosaic and Bragg intensity

A typical example of the neutron scattering pattern at zero field is shown in Fig. 1. The map demonstrates the coexistence of four major diffraction peaks originating from two different types of helix domains with the wave vector along the $[111]$ and $[11\bar{1}]$ axes. The observation of several peaks is caused by a large mosaic of the *magnetic* rather than the crystallographic structure of MnSi. The mosaic of the magnetic structure was determined by measuring the rocking curve of the magnetic reflection at $\mathbf{q}=\mathbf{k}$ parallel to $[111]$ (Fig. 2). The full width half maximum (FWHM) at $H=1$ mT is of order of 1.7° being much bigger than that of the crystallographic structure (0.2°) and is almost equal to the value of the Bragg angle (1.8°). Thus, it becomes clear that if the Bragg condition is ideally fulfilled for one reflection then it is also fulfilled partially for the other reflections. The value

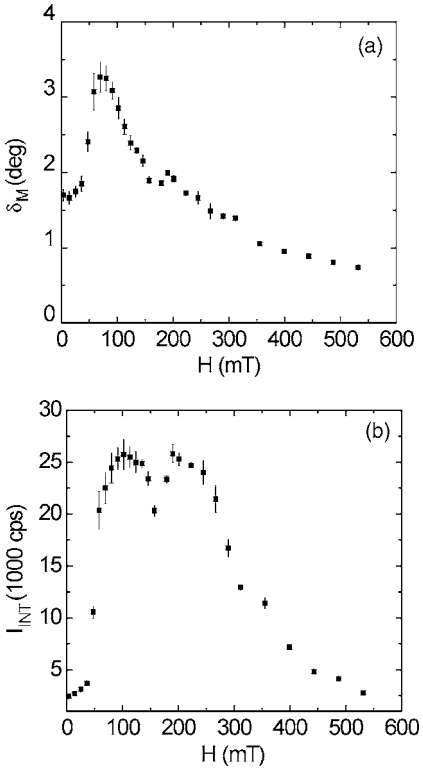

FIG. 3. The magnetic mosaic δ_M (a) and the integral intensity I_{int} (b) of the magnetic Bragg reflection $(\xi\xi\xi)$ as a function of the applied field. The data is not corrected for resolution.

of the magnetic mosaic in zero field does not change with temperature from 10 K to T_C.

The magnetic structure of MnSi under applied field has a complicated and irreversible behavior at $T<T_C$. Therefore, it is important that the magnetic history of the sample is always uniquely defined. We performed the measurements in the following way: (i) zero field cooling from the paramagnetic state to the temperature of interest T; (ii) raising the field from $H=0$ to the field of interest; and (iii) the field direction is fixed with respect to the sample in the rocking scan experiment. Using these principles the rocking curves of the Bragg peak (111) were taken at different values of the field at $T=15$ K (Fig. 2). The curves are well fitted by the Gaussian function:

$$I(\phi)=I_{BG}+\sqrt{\frac{2}{\pi}}\frac{I_{int}}{\delta_M}\exp\left(-2\frac{(\phi-\phi_c)^2}{\delta_M^2}\right), \tag{8}$$

where I_{BG} is a the background intensity. The integral intensity I_{int}, the center of the Gaussian ϕ_c, and the FWHM, or mosaic of the helix structure δ_M, were obtained from the fit.

Figure 3(a) shows δ_M as a function of the field. It reaches a maximum at $H=70$ mT and then decreases exponentially to the resolution level that is of the order of 0.75°. The field dependence of the integral intensity I_{int} is shown in Fig. 3(b). It is small at low H, then it increases sharply at $H_{C1}=70$ mT, and decreases again diminishing to zero at $H_{C2}=570$ mT, where the conical structure transforms to a ferromagnetic alignment.

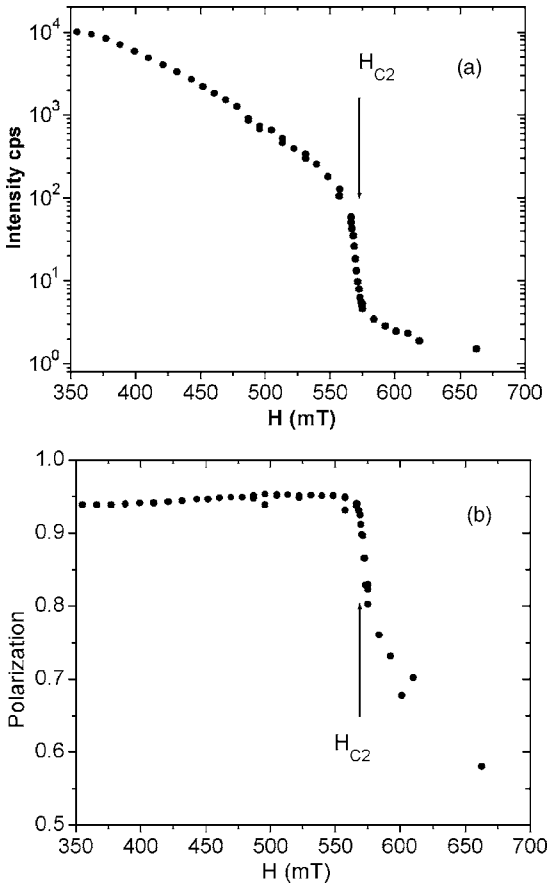

FIG. 4. The field dependence of the integral intensity (a) and the polarization (b) of the diffraction peak ($\xi\xi\xi$) for $\mathbf{H}\|\mathbf{P}\|[111]$ at $T=15$ K.

There are three features in Figs. 3(a) and 3(b) at H_{C1}, H_{C2}, and H_{in}. The sharp increase of the integral intensity of the reflection (111) at H_{C1} is accompanied by the decrease of the intensity of the reflections $(11\bar{1})$, $(1\bar{1}1)$, $(\bar{1}11)$ as well as by the increase of the magnetic mosaic. This is interpreted as a reorientation of the helices with the wave vector along the three unfavorable axes $([11\bar{1}],[1\bar{1}1],[\bar{1}11])$ to the favorable axis with the wave vector $\mathbf{k}$ along the $[111]$ axis.

To specify the behavior of the helix near H_{C2} the intensity and the polarization of the Bragg reflection (111) were measured in detail and are plotted as a function of field in Figs. 4(a) and 4(b), respectively. The polarization is constant and is equal to 1 in the whole field range $H<H_{C2}$. The value of the helix wave vector $\mathbf{k}$ does not change with the magnetic field. The abrupt change of the intensity and polarization at H_{C2} shows that the transition to the ferromagnetic state is sharp in contradiction to the simple classical theory,[21] which predicts the second order transition with $I_{int}\sim\sin^2\alpha=(H_{\|}/H_{C2})^2$. The constant polarization at $H<H_{C2}$ shows clearly that the chirality of the spin structure does not change at all. As the system undergoes the transition to the field induced ferromagnetic state, the static spiral structure disappears but the polarization-dependent scattering is still observed. According to the theory[21] it is the spin-wave scattering, which is maximal at the former helix vector $\mathbf{Q}=\mathbf{k}$. This

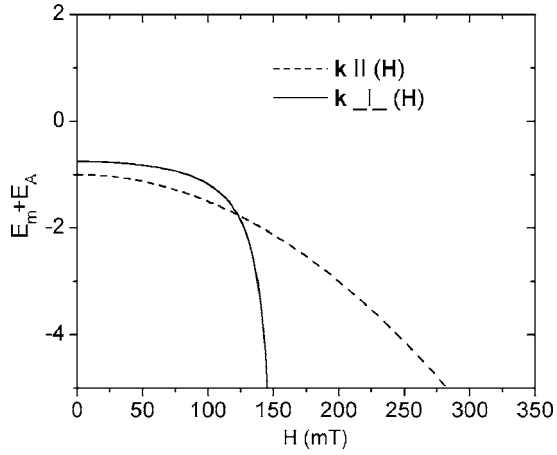

FIG. 5. Orientation dependence of the free energy (sum of the anisotropy and the magnetic energy) as a function of the field for the helix wave vector along the field direction [111] and perpendicular to it for parameters $H_{C2}=570$ mT and $\Delta=g\mu_B H_{in}=12$ μeV.

scattering has an unusual form as we have now two sources of the spin chirality: the magnetic field and the DM interaction. [See Eq. (72) in Refs. 21 and 30]. As a result the ω-integrated chiral part of the intensity is an odd function of vector $\mathbf{q}$ determined as difference $\mathbf{q}=\mathbf{Q}-\mathbf{k}$, where $\mathbf{Q}$ is the momentum transfer: $I_{int,ch}(\mathbf{q})=-I_{int,ch}(-\mathbf{q})$ whereas the conventional part of the I_{int} is the even function of $\mathbf{q}$. Hence we have partial cancellation of the chiral part of the intensity measured along the vector $\mathbf{k}$ and a decrease of the polarization above H_{C2}. Unfortunately, an exact treatment of the data at $H>H_{C2}$ is hardly possible because of the low signal-to-noise ratio.

The third feature concerns the fact that the integral intensity I_{int} has a well-pronounced minimum at $H_{in}\simeq 160$ mT. It demonstrates an instability of the helix structure in the narrow region near H_{in}. We explain this instability in terms of a competition between the magnetic energy of the system and the anisotropy energy. In our case H_{in} is less than $H_{C2}\simeq 570$ mT and parameter of the theory $\sin^2\alpha_{in}=(H_{in}/H_{C2})^2\simeq 0.08\ll 1$. In this case from Eqs. (2) and (4) for the free energy we have

$$E(\mathbf{k},\mathbf{H})=f_{an}^0\sum\hat{c}_i^2(\hat{a}_i^2+\hat{b}_i^2)-\frac{Sh_{\|}^2}{2h_{C2}}-\frac{Sh_{\perp}^2\Delta^2}{h_{C2}(\Delta^2-h_{\perp}^2/2)},\tag{9}$$

where $f_{an}^0<0$ and $\Sigma\hat{c}_i^2(\hat{a}_i^2+\hat{b}_i^2)$ has its maximal value 2/3 if $\mathbf{k}\|\mathbf{H}\|[111]$. In this case $h_{\perp}=0$ and the last term in Eq. (9) is zero. For other directions of the wave vector $\mathbf{k}$ this term becomes very important and at $h_{\perp}\to\Delta\sqrt{2}$ the energy with $\mathbf{k}\perp\mathbf{H}\|[111]$ becomes smaller than that with $\mathbf{k}\|[111]\|\mathbf{H}$. So the helix axis $\mathbf{k}$ has to turn perpendicular to the field. Figure 5 shows the schematic behavior of the free energy as a function of the field for two possible orientations of the helix wave vector. We take the values of the free parameters close to the values as extracted from the experiments: (i) gap $\Delta\simeq g\mu_B H_{in}/\sqrt{2}=12$ μeV and (ii) the critical field h_c

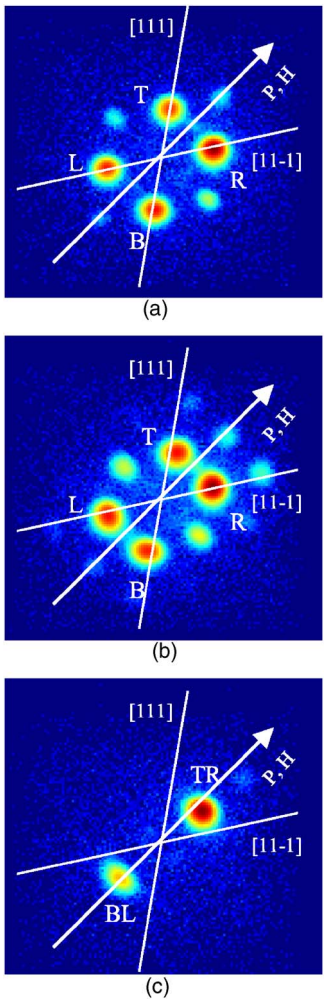

FIG. 6. (Color online) Contour maps of the diffraction peaks on a logarithmic scale for $T=10$ K for $\mathbf{H}\|\mathbf{P}\|[110]$. (a) $H=1$ mT, (b) $H=50$ mT, and (c) $H=150$ mT.

$=570$ mT. It is seen from Fig. 5 that for $\mathbf{k}$ along the field, the free energy decreases proportionally to $-h^2$, while $E_{\mathbf{k}\perp\mathbf{h}}$ decreases faster with increasing field. At an intermediate field determined by the condition $E_{\mathbf{k}\|[111]\|\mathbf{h}} \approx E_{\mathbf{k}\perp\mathbf{h}}$, the magnetic spiral destabilizes. This instability takes place up to $h \simeq \Delta\sqrt{2}$. However, at $h_\perp > \Delta\sqrt{2}$ the denominator in the last term becomes negative. As was shown in, Ref. 21 this denominator is the square of the spin-wave gap and when it is negative the system is instable. Hence it has to return to the $\mathbf{k}\|\mathbf{h}\|[111]$ state. Such two rotations were observed near the same field $H_{in} \simeq 160$ mT just below T_c.[20] At low T the region of this instability is very narrow and we see the minimum only in Fig. 3(b). It should be noted also that the last term in Eq. (9) is a result of approximations which do not work at $h_\perp$ very close to $\Delta\sqrt{2}$.[21]

B. Rotation of the helix vector k

To illustrate the typical behavior of the magnetic spirals in a magnetic field that deviates from the [111] axis we show in Fig. 6 experimental results for H along the [110] direction. The intensities of the diffraction peaks are given on a logarithmic scale. The contour map at $H=0$ and $T=10$ K shows four major and three minor peaks [Fig. 6(a)]. The four major peaks (closest to the center) are reflections attributed to helices with wave vectors that are collinear with the [111] and $[11\bar{1}]$ directions. We denote these peaks as left (L), bottom (B), right (R), and top (T) ones in accordance with their positions in Fig. 6(a). Additional small peaks at $\mathbf{q}=\mathbf{q}_R+\mathbf{q}_B$, $\mathbf{q}=\mathbf{q}_R+\mathbf{q}_T$, $\mathbf{q}=\mathbf{q}_L+\mathbf{q}_B$ and $\mathbf{q}=\mathbf{q}_L+\mathbf{q}_T$ are the result of double Bragg scattering. When a small magnetic field $H=50$ mT is applied, new peaks appear at $\mathbf{q}=2\mathbf{q}_L$, $\mathbf{q}=2\mathbf{q}_R$, $\mathbf{q}=2\mathbf{q}_T$, and $\mathbf{q}=2\mathbf{q}_B$ [Fig. 6(b)]. All peaks move toward the direction of the magnetic field, i.e., the direction of the helix vectors $\mathbf{k}$ changes, however, the value of $|k|$ remains constant. When the field exceeds $H=120$ mT, the peaks almost collapse along the direction of the magnetic field $\mathbf{k}\|\mathbf{H}$, and finally two peaks are left on the contour map [Fig. 6(c)].

The integral intensities for the T and R, and L and B peaks are shown in Figs. 7(a) and 7(b), respectively, as a function of the magnetic field. The polarization of the peaks is presented in Fig. 7(c). The position of the peaks is determined by the angle between the direction of spirals and of the magnetic field $\mathbf{H}$. This angle for two spirals being initially separated and then united is shown in Fig. 7(d).

Figure 7 shows that upon increasing the magnetic field from 1 to 70 mT, the intensity of the peaks increases. This result reflects the progressive reorientation of the helices with $\mathbf{k}$ along the $[1\bar{1}1]$ and $[\bar{1}11]$ axes (invisible in the experiment) along the [111] and $[11\bar{1}]$ axes as observed in Fig. 6. In the range of H from 0 to 120 mT all peaks rotate toward the field direction and the polarization of the peaks increases to the saturation value. The change in polarization of the peaks is related to the movement of the peaks toward the field direction. It is well described by Eq. (7) $P=P_0\cos(\phi_{\text{exp}})$. Thus the calculated value of the polarization with ϕ_{exp}, shown in Fig. 7(d), is close to the experimentally measured value of the polarization [Fig. 7(c)].

In the field range $H \sim 120$ mT peaks collapse to the direction of the magnetic field. The pairs of peaks on the right- and left-hand side of the detector collapse into single peaks, respectively. The intensity of these united peaks decreases strongly with further increase of the magnetic field. It is caused by movement of the $\mathbf{k}$ vector away from the Bragg condition under applied field due to the misalignment of the field with the Bragg condition since $\mathbf{k}\|\mathbf{h}$. The polarization of the peaks decreases slightly what is connected to the fact that the signal-to-noise ratio dramatically decreases. When the amplitude of the magnetic field is decreased, the data shows a significant hysteresis in the intensity. Peaks become separated again near $H=70$ mT. The intensity of the peaks after manipulation with magnetic fields differs from the intensity before it.

When the field $\mathbf{H}$ is applied along the [001] axis, the magnetic helix shows a similar behavior as along the [110] axis. The map in Fig. 8(a) shows Bragg reflections and the direction of the magnetic field for $\mathbf{H}\|[001]$: (1) four major peaks at $\mathbf{q}_R$, $\mathbf{q}_L$, $\mathbf{q}_T$, and $\mathbf{q}_B$ are denoted as left (L), bottom (B), right (R), and top (T); (2) Bragg peaks at $\mathbf{q}=\mathbf{q}_R+\mathbf{q}_B$, $\mathbf{q}=\mathbf{q}_R+\mathbf{q}_T$, $\mathbf{q}=\mathbf{q}_L+\mathbf{q}_B$, and $\mathbf{q}=\mathbf{q}_L+\mathbf{q}_T$ are due to the double Bragg scattering; and (3) the second harmonic peaks appear

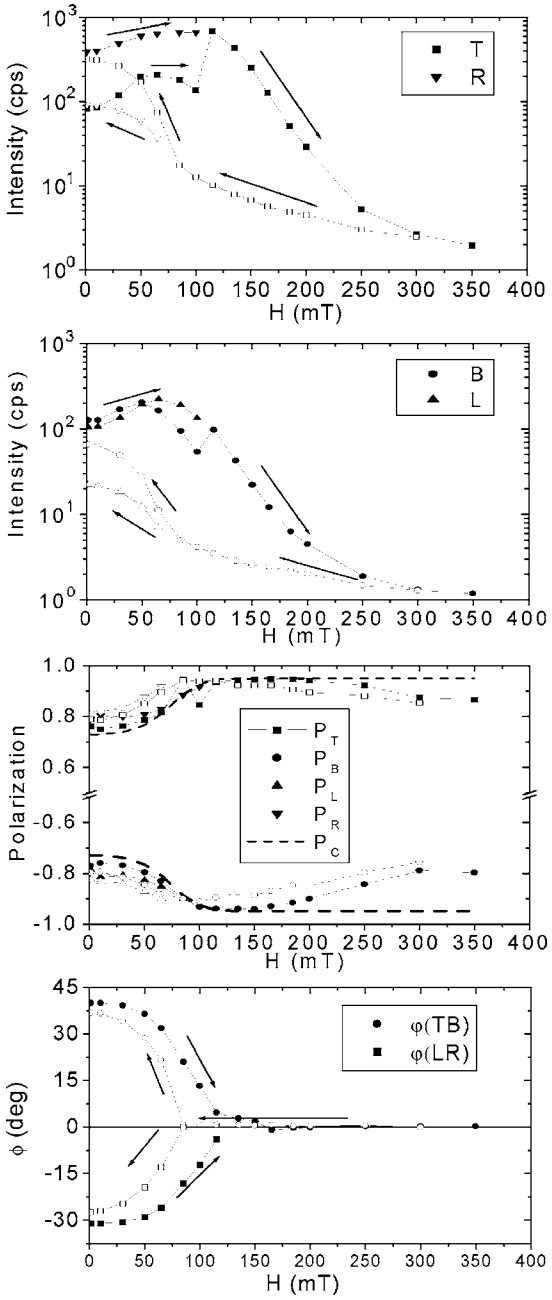

FIG. 7. Magnetic field dependence of (a) the integral intensity of the L and R peaks corresponding to the axis [111]; (b) the integral intensity of the B and T peaks, corresponding to the axis $[11\bar{1}]$; (c) the polarization of these peaks; and (d) the angle of their rotation for $\mathbf{H}\|[110]$ at $T=10$ K.

at $2\mathbf{q}_T$, $2\mathbf{q}_R$, and $2\mathbf{q}_B$. All these peaks are the reflections from two helices with wave vectors along the [111] and the $[11\bar{1}]$ axes.

The field dependence of the angle determining the positions of the peaks for these two helices is shown in Fig. 8(b). It is seen that the reorientation develops in two steps with increasing field. First, when H grows from 0 mT to 130 mT, the peaks rotate toward the field direction, so that a direction of the helix vectors $\mathbf{k}$ changes but their amplitudes $|k|$ are constant. When the field exceeds $H=130$ mT, the peaks (helix axis) collapse to the line along the field direction $\mathbf{k}\|\mathbf{H}$, so that only two peaks are left on the contour map. Upon decreasing field, again a small hysteresis loop of 20 mT in the rotation angle is observed. Peaks become separated again at the field $H=110$ mT.

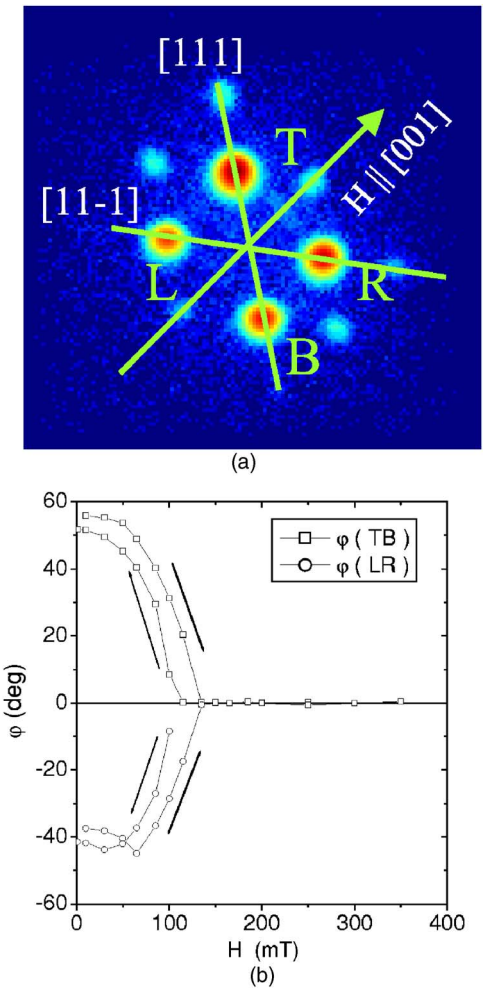

FIG. 8. (Color online) Magnetic field dependence of the angle of the helix rotation for $\mathbf{H}\|[001]$ at $T=10$ K. (a) Shows the contour map of the diffraction peaks on a logarithmic scale for a field $H=1$ mT. (b) Rotation angle of the helix.

The $\mathbf{k}$-rotation effect is well interpreted in terms of the competition between the anisotropy and the magnetic energy. It is interesting to note that the second term in the magnetic energy [Eq. (4)] that is related to the spin wave gap Δ can be neglected for explaining the $\mathbf{k}$-rotation effect since $h_\perp = h \sin\phi \to 0$ when $\mathbf{k}$ rotates toward $\mathbf{h}$, i.e., $\phi \to 0$. Then the magnitude of the anisotropic interaction can be evaluated as $S^2Fk^2/6 \sim Sh_{col}^2/2h_{C2} \approx 1.8$ μeV, where h_{col} is the field value when peaks collapse onto the field direction. The result of the corresponding calculations will be published elsewhere.

C. Second harmonic induced by a perpendicular field

In the previous subsection we have pointed out the appearance of second harmonic Bragg peaks arising at $\mathbf{q} = \pm 2\mathbf{k}$ when the magnetic field is applied along the [110] or

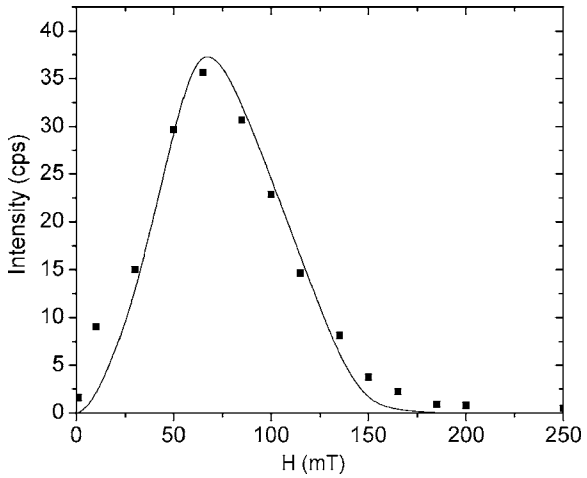

FIG. 9. Magnetic field dependence of the integral intensity of the second harmonic peak for $\mathbf{H}\|[110]$ at $T=10$ K. The line represents the calculated behavior according to Eq. (6).

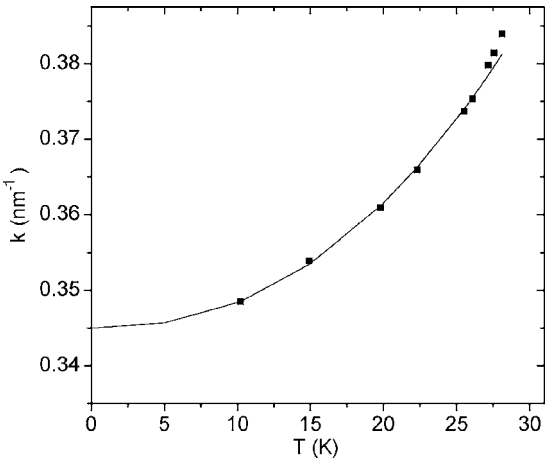

FIG. 10. Temperature dependence of the helix wave vector **k** at $H=1$ mT. The solid line corresponds to the fit as described in the text.

[001] directions, i.e., when **H** has a component perpendicular to **k**. It is important to note that no additional Bragg reflections appear, when the helix wave vector **k** is parallel to the magnetic field, i.e., when $\mathbf{H}\|[111]$. This demonstrates the deformation of the helix structure, i.e., an additional circular rotation of the spins in the same plane but with wave vector $2\mathbf{k}$ and constant magnetization along **H**.[21]

Figure 9 shows the intensity of the second harmonic as a function of the field. The solid line was calculated by using Eq. (6) with $h_\perp = h \sin\phi$ and shows good agreement with the data. The values of the free parameters were chosen to be close to the experimental conditions: the gap $\Delta=12$ μeV and the critical field $H_{C2}=590$ mT. $h_\perp = h \sin\phi$ was calculated using the experimentally measured value of the angle ϕ between the helix wave vector **k** and the field **h**. In this case the factor $[\Delta^2/(\Delta^2-h_\perp^2)]^2$ in Eq. (6) can be replaced by unity as $h_\perp = h \sin\phi \to 0$, and the factor $(h_\perp/h_{C2})^2$ determines the behavior of the cross section for the second harmonic.

V. TEMPERATURE EVOLUTION

As was shown above, the magnetic field changes the spin structure significantly. One can extract the following parameters of the spin structure from the diffraction experiments: the spiral wave vector **k**, the characteristic fields H_{C1}, H_{C2}, and H_{ins}. The temperature dependence of the helix wave vector length k is shown in Fig. 10. It is well described by the expression

$$k = k(0)[1 + a(T/T_C)^x] \tag{10}$$

with $k(0)=0.345\pm0.002$ nm, $a=0.11\pm0.01$, and $x=2.32\pm0.01$ for temperatures $(T_C-T)/T_C>0.1$. Our results are close to those obtained in Ref. 32.

The dependence of the critical fields H_{C1}, H_{C2}, and H_{in} on temperature is shown in Fig. 11. We fitted the experimental points to the expression

$$H_{Ci}(T) = H_{Ci}^0[1 - \alpha(T/T_C)^x], \tag{11}$$

$i=1,2$. For the lower critical field H_{C1} the parameters of the fit are: $H_{C1}^0=85\pm5$ mT; $\alpha_1=0.70\pm0.05$, and $x=2.5\pm0.1$. An important conclusion is that the temperature, as it increases, approaches the energy of the domain walls. If this would happen, one could observe the magnetic transition with a direction of the spiral structure **k** as an order parameter. In reality such a transition takes place only at $T\sim T_C$, when the satellite reflections are transformed into a ring of the intensity with constant $|k|$ (Ref. 31).

For the upper critical field H_{C2} the parameters of the fit are: $H_{C2}^0=600\pm10$ mT; $\alpha_2=0.30\pm0.02$, and $x=2.5\pm0.1$. As shown in Eq. (3), the critical field H_{C2} is related to the spin wave stiffness A through the wave vector **k**. Accordingly, the temperature dependence of the spin wave stiffness can be calculated from $H_{C2}(T)$ as $A(T)=A_0[1-c(T/T_C)^z]$ with $A_0=(d_0/2\pi)^2 H_0=50$ meV Å^2, $c=0.035\pm0.006$, and $z=2.4\pm0.1$. The obtained values for $A(T)$ are close to those obtained by three-axis spectroscopy: (1) for $T=5$ K the measured value of $A_m=50$ meV Å^2 (Ref. 2), and the estimated value $A_{est}=49$ meV Å^2; (2) for $T=25$ K the measured value

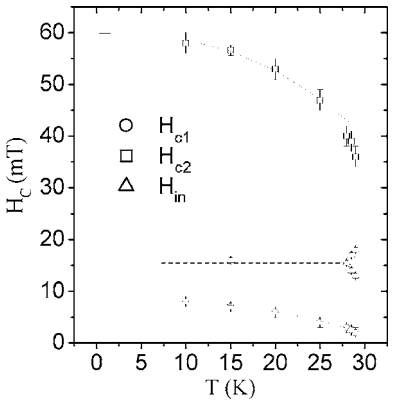

FIG. 11. Temperature dependence of the critical magnetic fields H_{C1}, H_{C2}, and H_{in} for $\mathbf{H}\|[111]$. The solid lines are fits to Eq. (12).

of $A_m = 23.5$ meV Å^2 (Ref. 33) and the estimated value $A_{est} = 33$ meV Å^2. The measurements of the SW stiffness mentioned above were performed at $H > H_{C2}$. The experimental study of the stiffness at low H has not been done yet. The theoretical considerations[21,34,35] predict a strongly anisotropic magnon dispersion at small H, i.e., in the helical phase.

The instability of the helix at $H_{in} = 160$ mT was measured at $T = 15$ K only. Nevertheless a similar effect of the same origin was observed near the critical temperature for fields $130 < H < 180$ mT. The maximal effect was detected at $H \approx 155$ mT (Ref. 20). These points are plotted in Fig. 11. This observation suggests that the instability is temperature independent.

VI. CONCLUDING REMARKS

The magnetic structure of a single crystal MnSi has been investigated by small angle polarized neutron scattering in a wide range of temperature and magnetic field. We have compared our findings with the theory recently developed for cubic magnets with the Dzyaloshinskii-Moriya interaction.[21] In this theory the ground state energy and the spin wave spectrum of magnetic compounds with the symmetry of MnSi is considered. It relates the existing interactions: isotropic exchange interaction A, Dzyaloshinskii-Moriya interaction D, anisotropic exchange interaction F, cubic anisotropy K, and the major parameters of the spin wave spectrum, such as the spin wave stiffness A and the spin wave gap Δ. The behavior of the helical structure and the spin-wave spectrum in magnetic field is considered also. The experimental results of this paper are in agreement with this theory.

Our experimental results are summarized in the following. The magnetic structure of MnSi in zero field consists of four left-handed spiral domains oriented along four $\langle 111 \rangle$ axes. A magnetic field, applied along one of the $\langle 111 \rangle$ axes, induces a single domain helix oriented along the field near H_{C1}. This reorientation is accompanied by a pronounced maximum in the magnetic mosaic of the spin structure. Thus the field H_{C1} determines the energy of the domain wall in the sample. The integral intensity of the Bragg reflection shows a sharp minimum at $H_{in} \approx 160$ mT. This phenomenon is well explained by the presence of a spin wave gap $\Delta \sim g\mu_B H_{in}/\sqrt{2}$ that provides the stability of the spin wave spectrum with respect to the perpendicular magnetic field. Two other features, i.e., the **k**-rotation effect and the second harmonic of the helix structure, take place when the field has a perpendicular component. These observations do not reveal directly the spin wave gap. However, they demonstrate the competition between the external magnetic field and the anisotropic exchange that is of the order of $S^2Fk^2/6$ and determines the orientation of the helix in the absence of a field. Further increase of the field leads to the magnetic phase transition from the conical to the ferromagnetic state near H_{C2}.

Finally, we demonstrate that the major interactions of the system can be estimated from diffraction experiments using the above mentioned theory.

(i) The magnetic phase transition from the conical to the ferromagnetic state at $H_{C2}(T)$ is observed. The critical field $H_{C2} \sim 600$ mT is related to the spin wave stiffness as $Ak^2 \approx g\mu_B H_{C2}$. We estimate the spin wave stiffness at $T = 0$ to be $A \approx 50$ meV Å^2 in agreement with its direct determination by neutron scattering.[2]

(ii).The temperature dependence of the wave vector $k = D/A \sim 0.035$ Å^{-1} is determined. Its value provides the DM characteristic energy $|Da| = A(ka) \approx 8$ meV Å^2. It is important to note that the scattering is fully polarized within the temperature range $T < T_C$ and within the field range $H < H_{C2}$. The polarization of the scattering satisfies the equation $P = (\hat{q}\mathbf{P}_0) = \cos\phi$, where ϕ is the angle between the incident polarization $\mathbf{P}_0$ and the scattering vector $\hat{q}$. This corresponds to the negative sign of the DM interaction. Neither temperature nor magnetic field are able to change this sign.

(iii) The **k**-rotation effect toward the field direction is observed when the field is applied along the $\langle 110 \rangle$ or $\langle 001 \rangle$ axes. The helix rotates toward and then collapses to the field direction at $H_{col} \sim 110$ mT. This field characterizes the weakest interaction of the system at $T = 0$, $S^2Fk^2/6 \sim Sh_{col}^2/2h_{C2} \sim 1.8$ μeV.

(iv) The integral intensity of the Bragg reflection shows a sharp minimum at $H_{in} = 160$ mT that is attributed to the instability of the helix structure and caused by the presence of a temperature-independent spin wave gap $\Delta \sim g\mu_B H_{in}/\sqrt{2} \approx 12$ μeV. This observation may be considered as the major result of the work since the presence of the gap may explain the quantum phase transition in MnSi at high pressure.

Indeed, two contributions to the spin wave gap have to be considered.[21] One contribution stems from the interactions between spin waves in presence of DM interaction $\Delta_{SW}^2 \sim Ak^2h_c/(4S) \sim (D^2/2A)^2$. The second contribution is determined by the cubic anisotropy, which is given by: $\Delta_{cub[111]}^2 \sim 3S^3Kh_c/2$. It is seen that Δ_{SW}^2 is always positive while Δ_{cub}^2 may have an arbitrary sign. So the different contributions to the gap may compete. Changing the sign and the strength of the cubic anisotropy, for example by pressure may lead to a quantum phase transition from the ordered to a spin-liquid state. It is a possible explanation of the transition that is observed in MnSi (Refs. 17–19).

ACKNOWLEDGMENTS

The PNPI-team acknowledges GKSS for their hospitality. The work is supported in part by the RFBR (Projects No 04-02-16342, 05-02-19889, and 06-02-16702) and the Russian State Programs "Neutron Research of Solids," "Quantum Macrophysics," and "Strongly Correlated Electrons in Semiconductors, Metals, Superconductors and Magnetic Materials."

[1] Y. Ishikawa, K. Tajima, D. Bloch, and M. Roth, Solid State Commun. **19**, 525 (1976).
[2] Y. Ishikawa, G. Shirane, J. A. Tarvin, and M. Kohgi, Phys. Rev. B **16**, 4956 (1977).
[3] I. E. Dzyaloshinskii, Zh. Eksp. Teor. Fiz. **46**, 1420 (1964).
[4] P. Bak and M. H. Jensen, J. Phys. C **13**, L881 (1980).
[5] D. Nakamishi, A. Janase, A. Hasejawa, and M. Kitaoka, Solid State Commun. **35**, 995 (1980).
[6] K. Koyama, T. Goto, T. Kanomata, and R. Note, Phys. Rev. B **62**, 986 (2000).
[7] K. Kadowaki, K. Okuda, and M. Date, J. Phys. Soc. Jpn. **51**, 2433 (1982).
[8] Y. Ishikawa and M. Arai, J. Phys. Soc. Jpn. **53**, 2726 (1984).
[9] C. Thessieu, C. Pfleiderer, A. N. Stepanov, and J. Flouquet, J. Phys.: Condens. Matter **9**, 6677 (1997).
[10] M. L. Plumer and M. B. Walker, J. Phys. C **14**, 4689 (1981).
[11] M. B. Walker, Phys. Rev. B **40**, 9315 (1989).
[12] S. V. Maleyev, V. G. Bar'jakhtar, and R. A. Suris, Fiz. Tverd. Tela (Leningrad) **4**, 3461 (1962) [S. V. Maleyev, V. G. Bar'yakhtar, and R. A. Suris, Sov. Phys. Solid State **4**, 2533 (1963)]; M. Blume, Phys. Rev. **130**, 1670 (1962).
[13] S. V. Maleyev, Phys. Rev. Lett. **75**, 4682 (1995); D. N. Aristov and S. V. Maleyev, Phys. Rev. B **62**, R751 (2000).
[14] G. Shirane, R. Cowley, C. Majkrzak, J. B. Sokoloff, B. Pagonis, C. H. Perry, and Y. Ishikawa, Phys. Rev. B **28**, 6251 (1983).
[15] M. Ishida, Y. Endoh, S. Mitsuda, Y. Ishikawa, and M. Tanaka, J. Phys. Soc. Jpn. **54**, 2975 (1985).
[16] B. Roessli, P. Böni, W. E. Fischer, and Y. Endoh, Phys. Rev. Lett. **88**, 237204 (2002).
[17] C. Pfleiderer, G. J. McMullan, S. R. Julian, and G. G. Lonzarich, Phys. Rev. B **55**, 8330 (1997).
[18] C. Pfleiderer, S. R. Julian, and G. G. Lonzarich, Nature (London) **414**, 427 (2001).
[19] C. Pfleiderer, D. Resnik, L. Pintschovius, H. Von Löhneysen, M. Garst, and A. Rosch, Nature (London) **427**, 227 (2004).
[20] S. V. Grigoriev, S. V. Maleyev, A. I. Okorokov, Yu. O. Chetverikov, and H. Eckerlebe, Phys. Rev. B **73**, 224440 (2006).
[21] S. V. Maleyev, Phys. Rev. B **73**, 174402 (2006).
[22] A. Zheludev, S. Maslov, I. Tsukada, I. Zaliznyak, L. P. Regnault, T. Masuda, K. Uchinokura, R. Erwin, and G. Shirane, Phys. Rev. Lett. **81**, 5410 (1998).
[23] A. Zheludev, S. Maslov, G. Shirane, I. Tsukada, T. Masuda, K. Uchinokura, I. Zaliznyak, R. Erwin, and L. P. Regnault, Phys. Rev. B **59**, 11432 (1999).
[24] M. E. Zhitomirsky and I. A. Zaliznyak, Phys. Rev. B **53**, 3428 (1996).
[25] T. A. Kaplan, Z. Phys. B: Condens. Matter **49**, 313 (1983).
[26] L. Shekhtman, O. Entin-Wohlman, and A. Aharony, Phys. Rev. Lett. **69**, 836 (1992).
[27] L. Shekhtman, A. Aharony, and O. Entin-Wohlman, Phys. Rev. B **47**, 174 (1993).
[28] O. Entin-Wohlman, A. Aharony, and L. Shekhtman, Phys. Rev. B **50**, 3068 (1994).
[29] B. Lebech, J. Bernhard, and T. Freltoft, J. Phys.: Condens. Matter **1**, 6105 (1989).
[30] There are misprints in this equation: in all terms there has to be a combination $\omega+i\delta$.
[31] S. V. Grigoriev, S. V. Maleyev, A. I. Okorokov, Yu. O. Chetverikov, R. Georgii, P. Böni, D. Lamago, H. Eckerlebe, and K. Pranzas, Phys. Rev. B **72**, 134420 (2005).
[32] B. Fak, R. A. Sadykov, J. Flouquet, and G. Lapertot, J. Phys.: Condens. Matter **17**, 1635 (2005).
[33] F. Semadeni, P. Böni, Y. Endoh, B. Roessli, and G. Shirane, Physica B **267-268**, 248 (1998).
[34] T. R. Kirkpatrick and D. Belitz, Phys. Rev. B **72**, 180402(R) (2005).
[35] D. Belitz, T. R. Kirkpatrick, and A. Rosch, Phys. Rev. B **73**, 054431 (2006).